ACS NANO

www.acsnano.org

ARTICLE

Labeling the Structural Integrity of Nanoparticles for Advanced In Situ Tracking in Bionanotechnology

Fabian Meder,*[,†,§] Steffi S. Thomas,[†,§] Laurence W. Fitzpatrick,[†] Amirah Alahmari,[†] Suxiao Wang,[‡] Jason G. Beirne,[‡] Gizela Vaz,[†] Gareth Redmond,[‡] and Kenneth A. Dawson*[,†]

[†]Centre for BioNano Interactions, University College Dublin, School of Chemistry and Chemical Biology, Belfield 4, Dublin, Ireland

[‡]Functional Nanomaterials, University College Dublin, School of Chemistry and Chemical Biology, Belfield 4, Dublin, Ireland

Supporting Information

ABSTRACT: **Observing structural integrity of nanoparticles is essential in bionanotechnology but not always straightforward to measure in situ and in real-time. Fluorescent labels used for tracking intrinsically nonfluorescent nanomaterials generally do not allow simultaneous observation of integrity. Consequently, structural changes like degradation and disassembly cannot easily be followed in situ using fluorescence signals. We show that thioflavin T (ThT), a fluorophore and molecular rotor known to tag specific fibril structures in amyloids, can "label" the structural integrity of widely used and intrinsically nonfluorescent, silica nanoparticles (SiNPs). Entrapment of ThT in SiNPs controls the fluorohphore's relaxation pathway and leads to a red-shifted fluorescence spectrum providing real time information on SiNP integrity. The dynamic change of ThT fluorescence during degradation of doped SiNPs is found much higher than that of common labels fluorescein and rhodamine. Degradation kinetics of core−shell structures recorded by ThT fluorescence and light scattering prove the capability to clearly distinguish structural features during SiNPs degradation and allow obtaining degradation kinetics in vitro, in biological media, in serum, and in cells. The effect is transferable to different types of materials, here shown for ThT incorporated SiNPs with tightly tailorable sizes (9−100 nm), poly(lactic-*co*-glycolic acid) (PLGA) nanoparticles, poly(9-vinylcarbazole) (PVK) nanoparticles, and iron-doped-SiNPs (FeSiNPs). We thus suggest molecular rotors such as ThT as additional labels to effectively and easily sense nanoparticle structural status in situ and to enhance understanding and development of programmed nanoparticle disassembly in bionanotechnology.**

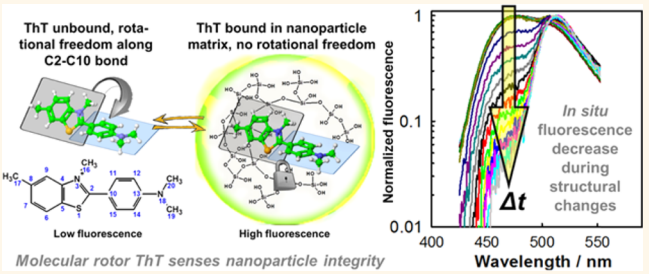

Molecular rotor ThT senses nanoparticle integrity

KEYWORDS: *bionano interactions, biodegradation, fluorescence labeling, core−shell nanoparticles, molecular rotors, differential centrifugal sedimentation, silica*

Nanoparticles are considered as multifunctional vehicles with great potential in bioscience, diagnostics, and in new therapies.[1,2] In biological surroundings, particles interact with biomolecules and are processed by cellular machineries which can lead to structural changes of the nanoparticles, partial and complete disassembly, or biodegradation.[3−6] Although this might be an intended or unwanted process, depending on the application, it is always a key parameter that requires careful observation. Tracking the nanoparticle structural integrity during different cascades of biological processing (cellular uptake, intracellular handling, transfer between different cells, etc.) is essential for targeted nanoparticle-cell interaction, nanoparticle biocompatibility, drug delivery, and general understanding of how organisms treat nanomaterials.[7−10] Observing structural integrity is analytically often difficult. For nanoparticles that have an intrinsic fluorescence, integrity can be easily followed in situ as fluorescence signals depend on material degradation status.[5] However, nanomaterials lacking an intrinsic fluorescence must be labeled with fluorescent molecules to track them effectively.[9,11−13] These labels generally do not reflect the particles' structural integrity.

SiNPs are intrinsically nonfluorescent and widely used due to their versatile synthesis routes and surface functionalizations, tailorable porosity, and so forth.[12,14−17] Doping SiNPs with, for example, iron[18] or calcium[19] is proposed for controlling biodegradability and bioaccumulation of SiNPs. Access to in situ information on integrity state of nanoparticles by

Received: February 8, 2016
Accepted: March 4, 2016
Published: March 9, 2016

DOI: 10.1021/acsnano.6b01001
ACS Nano 2016, 10, 4660−4671

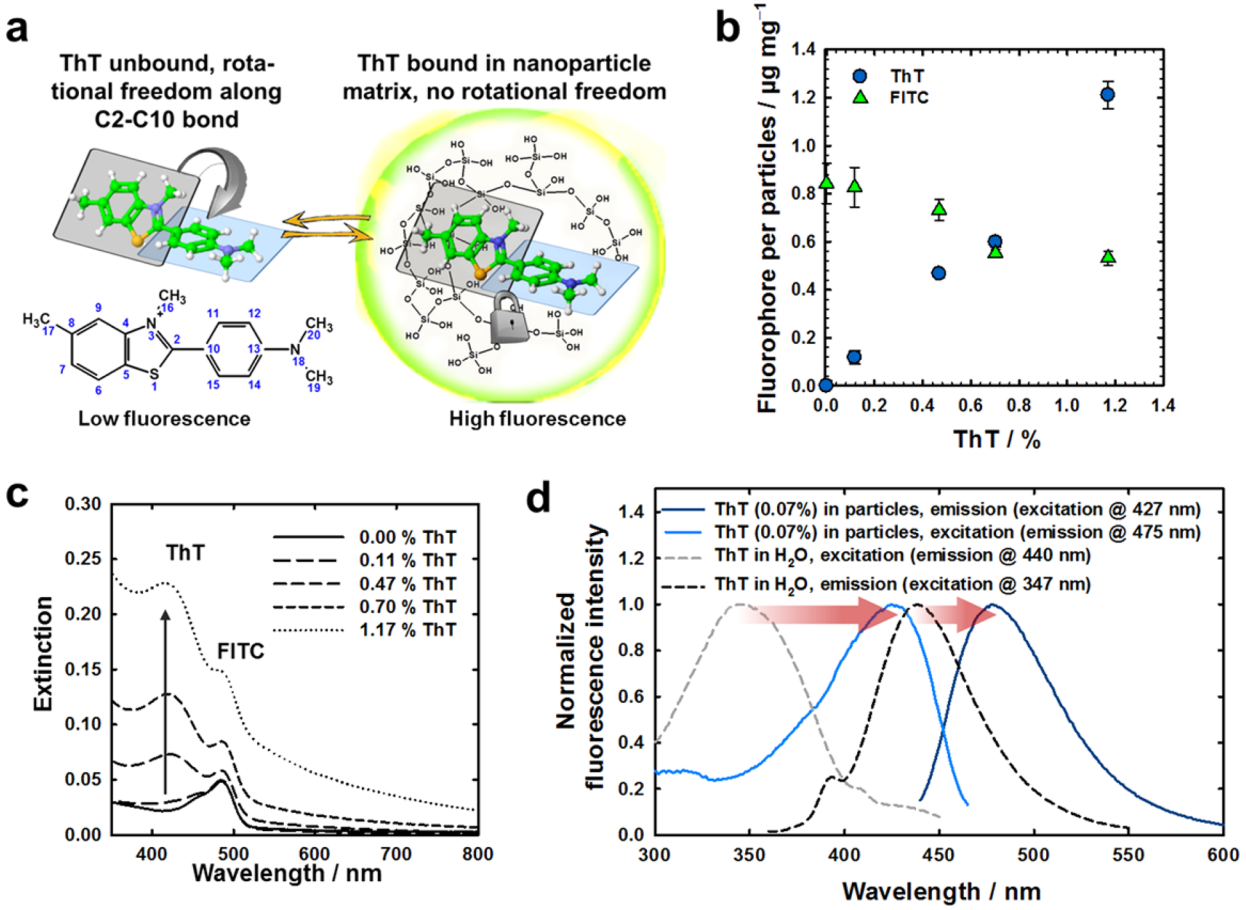

Figure 1. (a) Schematic representation of hypothesis on ThT fluorescence when unbound and bound in nanoparticles: Rotational freedom at C2−C10 bond of unbound ThT in solution results in low fluorescence at excitation/emission at ~430/475 nm. We hypothesize that rotational freedom is lost when ThT is incorporated into silica matrix, leading to high fluorescence signals at ~430/475 nm, a behavior known for ThT binding to amyloids.[27] (b) Resulting ThT and FITC doping concentrations in SiNPs in micrograms per milligram of particles. Data is plotted against ThT concentration used for synthesis in percent by weight related to tetraethyl orthosilicate (FITC concentration was kept constant at 0.03 wt %). (c) UV−vis spectra of SiNPs doped with ThT and FITC as in (b) showing characteristic peaks for ThT and FITC. The ThT peak increases expectedly the more ThT is added to the particles. (d) Fluorescence excitation and emission spectra of ThT after incorporation into SiNPs and unbound ThT in water. When ThT is incorporated in the SiNPs, a strongly red-shifted fluorescence spectrum is observed confirming the hypothesis of (a).

fluorescence microscopy and spectroscopy would be highly profitable for such developments. Fluorescein isothiocyanate (FITC) or rhodamine isothiocyanate (RITC) are often successfully used for tracking SiNPs by incorporation of the fluorophores into the silica matrix,[11,12,20] but fluorescence intensity variations observed after incorporation do not give information on particle integrity. It can be furthermore difficult to distinguish dissociated dye from degraded particles in a biological surrounding.[21] Observing structural changes and degradation in vitro and intracellular thus is often only possible ex situ and not in real-time. It requires moreover complex techniques such as elemental analysis or electron microscopy of cell components.[22,23] A promising approach for the difficult task of in situ monitoring integrity is dual or multiple labeling of different nanoparticle compartments. By labeling nanoparticle core and shell with two different labels—recent studies used either two different fluorescent dyes[9,24] or two different radionuclide labels[9,10]—nanoparticle degradation has been investigated in vitro and in vivo. When the two labels change their location individually, particle and shell must have separated due to particle degradation. However, if the nanoparticle and shell degrade and the released labeled molecules or ions remain in a similar location, degradation cannot be determined and is always limited to the spatial resolution of detection of the two signals, for example, by fluorescence microscopy or positron emission tomography.

Thus, it is beneficial to create a signal that responds directly to nanoparticle structure to understand processes on biomolecular and cellular level. Fluorescent molecular rotors have an intramolecular rotational axis and their fluorescence depend on the rotation around this axis. They have great potential to detect chemical and mechanical changes in their surrounding and have been used as viscosity probes or to detect membrane stress in polymers.[25] As a function of the rotational angle, a specific relaxation pathway can be opened or locked which influences the fluorescent profile. The rotation thereby depends strongly on the microenvironment of the molecule and changes in the surrounding lead to an alteration of fluorescence properties and thus can be sensitively detected. The sensitive fluorescence response toward rotational changes suggests locking molecular rotors within nanoparticles in a specific rotational state leading to a specific fluorescence profile. Upon alteration of the microenvironments, for example, by particle degradation, the rotational properties and fluorescence

DOI: 10.1021/acsnano.6b01001
ACS Nano 2016, 10, 4660−4671

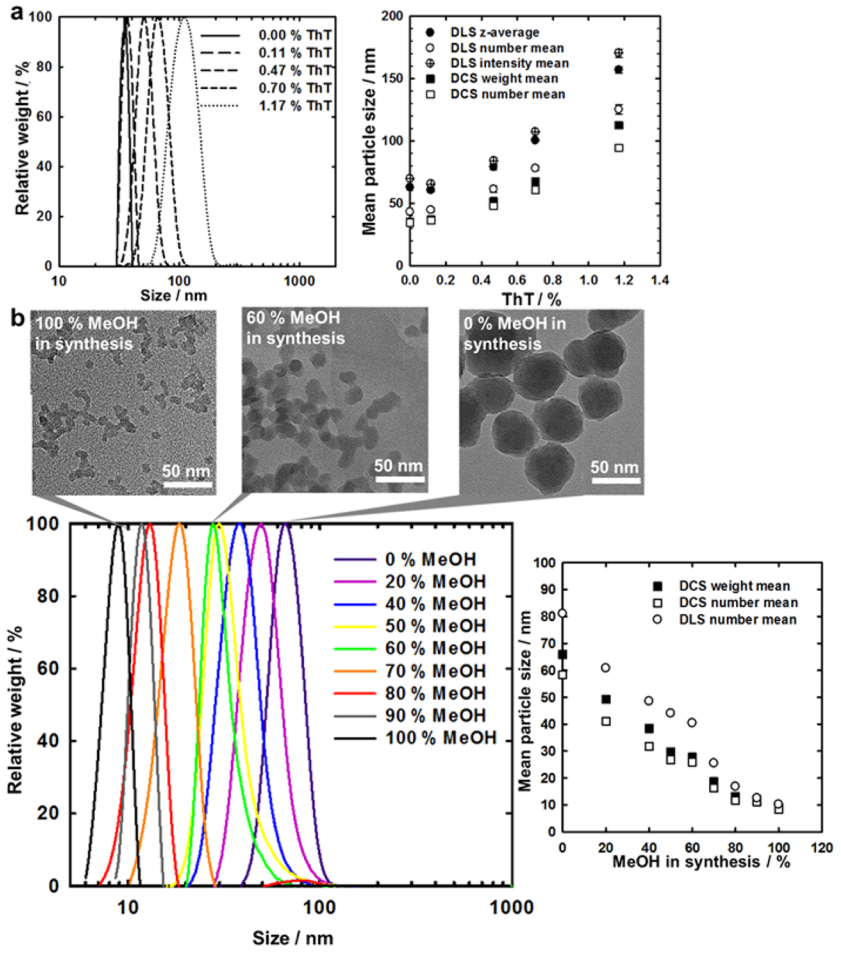

Figure 2. (a) SiNPs' particle size increases in correlation with added ThT amount measured by DLS and DCS. (b) Controlling SiNP size with constant ThT doping (0.7 wt %) is possible by varying methanol (MeOH) concentration in synthesis, measured by DCS, DLS and TEM (UV−vis, fluorescence spectra, and ThT and FITC loading of SiNPs synthesized using MeOH concentrations are given in the Figure S3). Size measurements of particles before growth of protective shell are shown.

emission would change providing in situ information on nanoparticle structural integrity. ThT is a fluorescent molecular rotor known to bind to toxic amyloids with the pharmacological interesting effect of reducing amyloid-associated toxicity.[26] While binding to amyloids, molecular rotation is inhibited and ThT establishes strong red-shifted fluorescence. Here, we report that ThT creates similar shifted fluorescence spectra upon entrapment in SiNPs, PLGA NPs, PKA NPs, and FeSiNPs based on inhibiting its molecular rotation in the particles and their integrity can be monitored sensitively and material-independently. New and sensitive ways of assessing nanoparticle integrity with a direct response and without spacial limitations will aid programming nanoparticle disassembly in situ, develop targeted drug delivery, and enhance understanding of the biological fate of engineered materials.

RESULTS AND DISCUSSION

ThT Incorporation in SiNPs: Effect on Spectral Properties and Particle Size. ThT is known to strongly change fluorescence properties when interacting with specific molecular structures, as those of protein fibrils in amyloids. Binding of ThT to the fibrils results in a large red shift of its excitation/emission (ex/em) spectra (from 385 to 450 nm and 445 to 482 nm, respectively)[27,28] resulting from its rotational molecular properties: In unbound state, the benzylamine and benzathiole rings of ThT can rotate around their shared carbon−carbon bond quenching excited states and lowering fluorescence emission (Figure 1a, left). However, in bound states, rotation is no longer possible preserving a specific relaxation pathway resulting in high quantum yields and shifted fluorescence maxima.[27,29] We aimed to use this property of ThT and to preserve its excited states by binding it into SiNPs (Figure 1a). ThT was incorporated into SiNPs in different concentrations by addition during synthesis without specifically covalently linking it. We furthermore included fluorescent dyes FITC or RITC as internal reference for ThT fluorescence and to obtain dual-labeled NPs that are compatible in different detection platforms. To increase stability of the dye-labeled core,[12,30] all particles are generally covered by a thin silica shell (~4 nm in case of ~60 nm particles, Figure S1) if not otherwise stated. Figure 1b shows amounts of ThT and FITC per mg SiNPs synthesized with variant ThT and constant FITC concentrations. UV−vis extinction spectra (Figure 1c) confirm the tailorable incorporation of ThT and FITC into SiNPs and show a concentration dependent absorbance peak with maximum at 430 nm indicating ThT incorporation. FITC absorbance can expectedly be observed at 490 nm.

ThT incorporation into the silica matrix leads to a distinct red shift of its ex/em maxima from 347 to 425 nm and 440 to 475 nm, respectively (arrows Figure 1d). ThT's red shift is

DOI: 10.1021/acsnano.6b01001
ACS Nano 2016, 10, 4660−4671

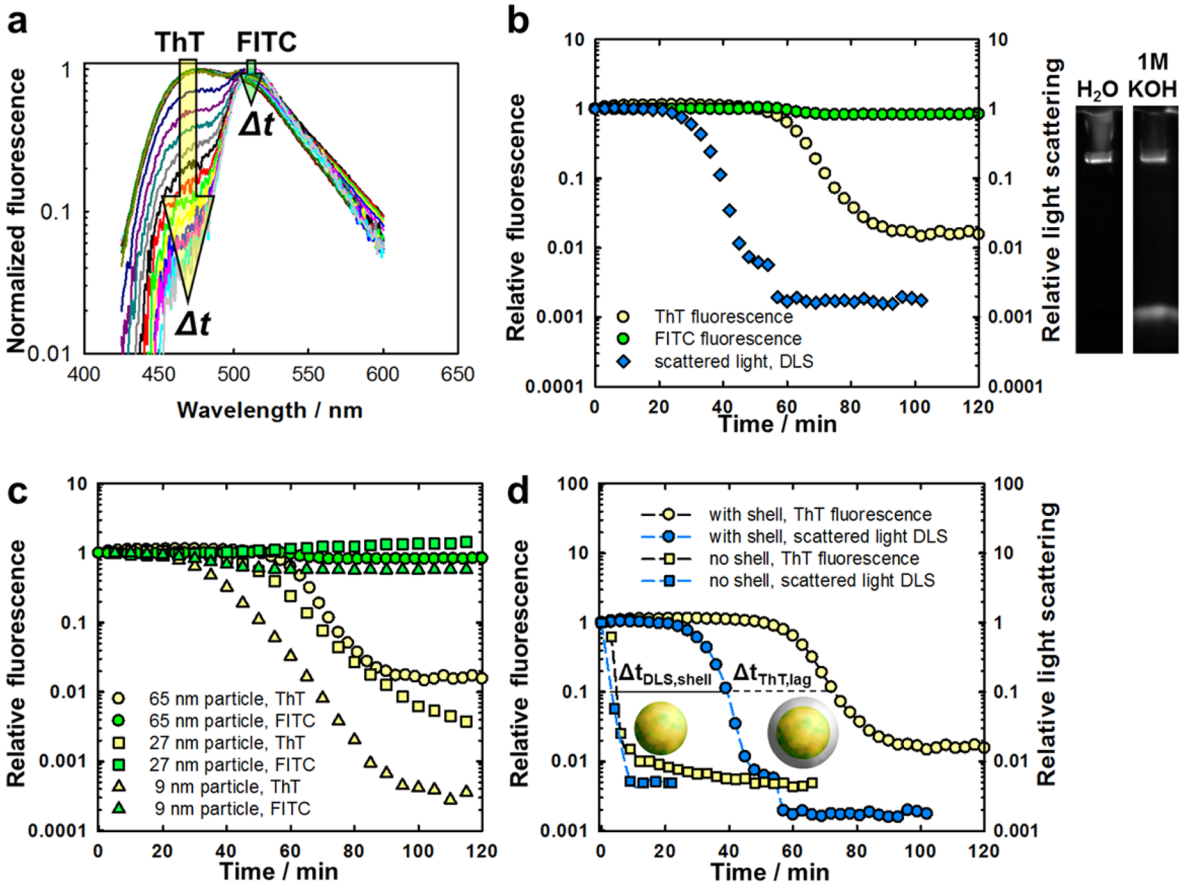

Figure 3. (a) Normalized fluorescence spectra of SiNPs during degradation upon continuous exposure to 1 M KOH for 120 min (excitation at 425 nm). ThT signal decreases strongly over time, whereas FITC signal varies only slightly. (b) SiNPs' ThT fluorescence drops during degradation upon continuous exposure to 1 M KOH (ThT, ex/em 410/475 nm and FITC, ex/em 475/520 nm). The relative fluorescence compares the fluorescence signal at time 0 with that during proceeding KOH exposure. Degradation is confirmed by reduction of light scattering obtained by DLS (blue squares) and gel electrophoresis (image on right-hand of graph). The gels show a single fluorescent band (FITC fluorescence) for SiNPs exposed to water (for 2 h), indicating no degradation. Gels for SiNPs exposed to 1 M KOH instead show a second band due to free molecules and particle debris that are able to diffuse into the pores of the gel upon degradation. (c) Degradation kinetics of differently sized SiNPs, determined using ThT fluorescence, showing that smaller SiNPs degrade expectedly faster. (d) Degradation kinetics of SiNPs with and without a protective shell measured by ThT fluorescence and light scattering; the shell delays the degradation (further characterization of particles given Figure S1). $\Delta t_{DLS,shell}$ and $\Delta t_{ThT,lag}$ were read out at 10-fold reduction of light scattering or fluorescent signal, respectively, and are discussed in the main text.

independent of the presence of FITC or RITC (Figure S2a) and the fluorescence intensity of the ThT signal at 475 nm is unaffected by the pH of the particle surrounding media (for pH 1−9, Figure S 2d and e). This suggests that the red shift originates of the microenvironment of ThT within the silica matrix. Entrapment and interaction seems to inhibit molecular rotation and to open a distinct relaxation pathway within the molecule resulting in the shifted emission spectra, similar to when it is bound in amyloids as hypothesized in Figure 1a (comparable red shifts are reported, see the first paragraph and ref 27). Responsible for effective incorporation of ThT into the silica matrix could be the positive partial charge at the nitrogen atom, which is in proximity to the rotational plane of the ThT molecule (Figure 1a) and might interact with anionic silicate species (e.g., $\equiv SiO^-$) widely present during sol-gel particle formation.[31] Additional fluorescent characterization is given in Figure S2 (influence of RITC and FITC on red shift, concentration dependent ThT fluorescence, fluorescence lifetime measurements, influence of pH on SiNP fluorescence).

ThT leads furthermore to a reproducible increase in particle size as a function of the added concentration (Figure 2a). Control toward smaller particle sizes down to 9 nm at a constant ThT concentration is achieved by altering nucleation size using different ratios of methanol/ethanol during synthesis.[32] This enables a series of highly monodisperse fluorophore-doped SiNPs with mean sizes from 9 to 100 nm (Figure 2b, dye loading and fluorescence spectra of these particles in Figure S3). We used differential centrifugal sedimentation (DCS) to measure particle size distributions in which the nanoparticles pass a density gradient during the measurement.[33] Sedimentation times in the gradient are recorded when particles pass an extinction detector employing a 405 nm laser. The detector signal depends on light scattering and absorbance of the SiNPs, which is generally low for silica due to transparency and especially low scattering for small SiNPs at the detector wavelength. However, when doped with ThT, the detectability of small and ultrasmall SiNPs was strongly increased due to increased absorbance at the detector wavelength. DCS is an essential technique in bionanoscience and further results and discussion on the effect are given in the Supporting Information Figure S4 and S5.

DOI: 10.1021/acsnano.6b01001
ACS Nano 2016, 10, 4660−4671

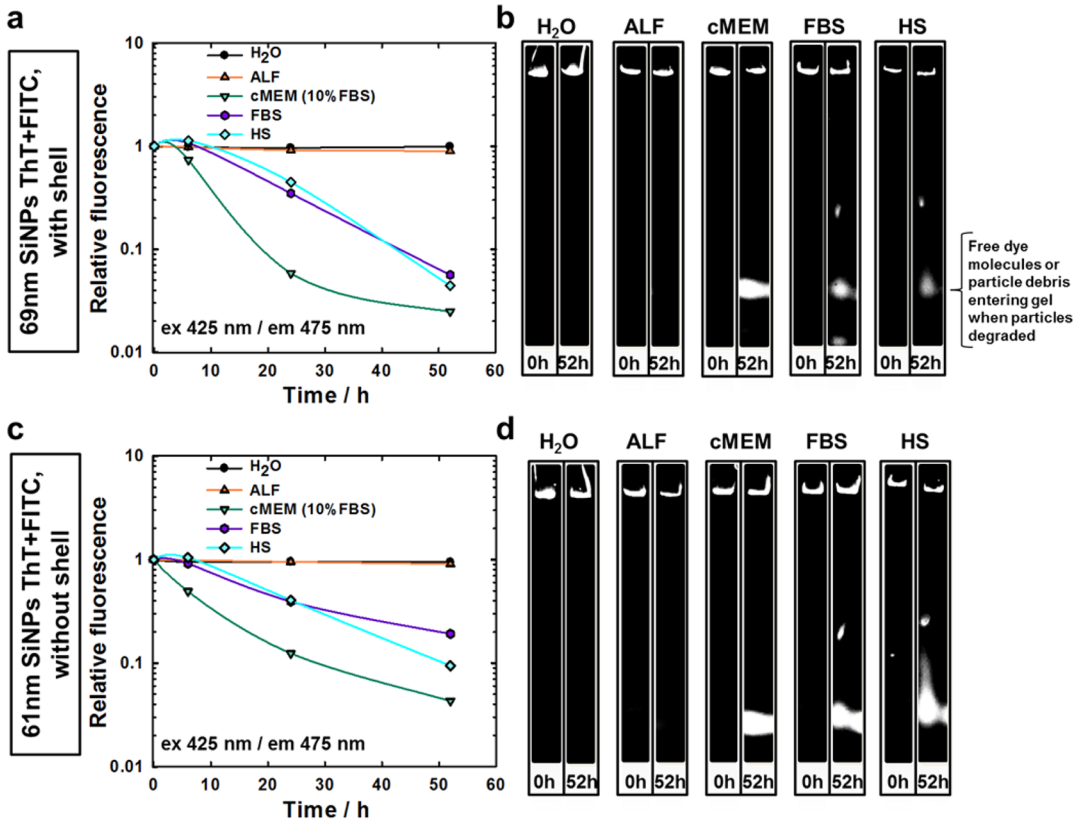

Figure 4. Degradation of SiNPs with and without shell in biological media during exposure for 52 h at 37 °C. (a) and (c) Relative ThT fluorescence decrease of SiNPs with and without shell, respectively, in cMEM, FBS, and HS suggesting degradation. ThT fluorescence remains stable in water and ALF suggesting no significant structural changes of the SiNPs (ex/em 425/475 nm). (b) and (d) Gel electrophoresis of SiNPs after 52 h exposure to the different media confirming the results obtained from ThT fluorescence. Upon degradation in cMEM, FBS, and HS, smaller particle debris and free fluorescent dye can enter the pores of the gel and can be seen as a second band at the bottom of the gel under illumination. Only one band is observed for SiNPs exposed to water or ALF suggesting no degradation. ALF (artificial lysosomal fluid), cMEM (Minimum Essential Medium containing 10% fetal bovine serum), FBS (fetal bovine serum), HS (human serum), reference (H_2O).

ThT Fluorescence during Structural Changes of the Nanoparticles: Degradation Kinetics. We assumed that as soon as the SiNPs suffer a change in internal structure, dissolve, or degrade, ThT may disassociate from the particle and regain rotational freedom resulting in a loss of fluorescence intensity at the shifted maxima. To test this hypothesis, SiNPs were degraded under controlled conditions using 1 M KOH and the fluorescent signal of ThT was recorded as a function of exposure time (Figure 3a,b).

SiNPs' ThT fluorescence showed a strong, time-dependent reduction following KOH exposure (Figure 3b). The signal is ~1000 times lower after 2 h of incubation when compared to beginning of the experiment. In contrast, neither FITC (Figure 3b) nor RITC fluorescence (Figure S6) varied in this extent; in fact, their fluorescence only slightly decreased. To verify the particle degradation, we measured the decrease in count rate of scattered light due to particle dissolution by dynamic light scattering (DLS, Figure 3b). Due to the proportionality of light scattering and particle radius, lower counts of scattered light overtime indicate that the particle size decreases, for example, by disassembly into smaller particles or by continuous "peeling-off" the particle surface. One can observe a lag between decay of ThT fluorescence and that of DLS signal that is expected to be due to the core−shell structure of the particles and will be discussed later. Gel electrophoresis after exposing particles to either H_2O or 1 M KOH moreover confirms degradation as due to degradation, smaller debris, and free fluorescent dye can enter the pores of the gel and can be observed under illumination as a second band at the bottom of the gel (inset in Figure 3b). Both techniques confirm the dissolution of SiNPs in 1 M KOH (Figure 3b). When performing the experiments in H_2O, the ThT fluorescence signal remains unchanged, excluding also any photo bleaching of ThT during the duration of the experiments (Figure S7). The influence of 1 M KOH on the fluorescence of the released, unbound ThT needs to be considered to exclude any artifacts resulting from the media effects on the dye. ThT fluorescence is about five times lower in 1 M KOH compared to water (Figure S8) as also found by Hackl et al. when ThT was exposed to acidic and basic pH.[34] The signal decrease upon particle degradation, however, resulted in a fluorescence decay of up to 1000 times (Figure 3b) and 2500 times (Figure 3c). We show later that single ThT molecules do not change fluorescence in biological media and show slight fluorescence increase at 475 nm in THF while a strong decrease of ThT fluorescence at 475 nm is observed when ThT-doped nanoparticles degrade in such media. This suggests that the major impact on ThT fluorescence at 475 nm is the particle matrix integrity, which surrounds ThT molecules and influences its molecular rotation and relaxation pathways. A reestablishment of the signal at ex/em 347/440 nm (blue shift) furthermore suggests the presence of free rotating ThT molecules upon particle degradation (Figure S9). The emission

DOI: 10.1021/acsnano.6b01001
ACS Nano 2016, 10, 4660−4671

decrease at 475 nm thus likely mirrors the transfer of the highly fluorescent locked molecular state of ThT into a state of increased molecular rotational freedom and thereby reflects particle integrity.

To furthermore prove the ability of ThT as a potential sensitive structural integrity sensor, we compared degradation kinetics of SiNPs as a function of particle size (Figure 3c). Smaller particles are expected to degrade faster due to the higher surface to volume ratio. This effect is reflected in the measured ThT fluorescence signals which start to decrease earlier for smaller and later for larger particles and degradation kinetics correlate expectedly with particle size.

To analyze the origin of the lag of ThT fluorescence decay compared to light scattering decay (Figure 3b) in detail, we compared degradation of particles with and without a 4 nm protective silica shell (Figure 3d). For core particles without shell, light scattering and ThT signal dropped almost synchronous, whereas lag is observed for core–shell particles. The lag between the ThT and DLS signal is thus likely due to the unlabeled shell of the particles which dissolves before the labeled core is affected. This is further confirmed by the following observations. For early degradation events (defined here as the time points when light scattering or ThT fluorescence is 10-fold reduced), we observe from light scattering that core–shell particles take ~36 min longer than core particles to reach this state ($\Delta t_{DLS,shell}$, Figure 3d). The time difference $\Delta t_{DLS,shell}$ corresponds almost exactly to the lag between DLS and ThT signal for core–shell particles, $\Delta t_{ThT,lag}$, which is ~34 min. It suggests that the DLS signal reflects the entire core–shell particle while the ThT fluorescence obviously mirrors only the ThT-labeled core. It agrees with the different nature of the signals. Although light scattering correlates with particle diameter due to Rayleigh scattering, ThT fluorescence correlates with the state of interaction between ThT and the silica matrix. To confirm this analysis, we delayed the degradation kinetics by recording SiNP degradation (without shell) at a lower KOH concentration (0.1 M, Figure S10). Light scattering and ThT fluorescence decreased simultaneously with a lag for both signals due to the lower KOH concentration. This further confirms "peeling-off" degradation mechanism occurs in which the shell offers itself before the dye-labeled core is dissolved due to lag between the DLS and ThT signal for SiNPs with shell. ThT fluorescence thus reflects and provides important information on the particle structure during degradation events.

Tracking ThT-Doped Nanoparticle Integrity In Situ in Biological Surroundings. We applied the same method to investigate the integrity of SiNPs over 48 h in biological media at 37 °C. Therefore, we used complete Minimum Essential Medium containing 10% fetal bovine serum (cMEM), as a typical cell culture media, artificial lysosomal fluid (ALF) simulating the acidic (pH 4.5) and ionic conditions found in lysosomes, fetal bovine serum (FBS), human serum (HS), and water as reference (Figure 4). ThT fluorescence pattern suggests that particle degrade in cMEM, FBS, and HS but remain in ALF (Figure 4a,c). The particles were furthermore analyzed by gel electrophoresis, which confirms degradation (Figure 4b,d). Using ThT separately (free ThT molecules in media), we proved that the media either did not influence ThT fluorescence or induced a slight fluorescence increase (Figure S11) thus confirming that the observed fluorescence decrease for ThT-doped SiNPs is due to particle degradation. Comparing ThT fluorescence of SiNPs with and without shell shows that the degradation in biological media is slightly delayed for SiNPs with shell (Figure S12), similar to the observation made when SiNPs degrade in 1 M KOH. Amorphous SiO_2 is usually stable against dissolution below pH 10.[35] Accordingly, in SiNPs in H_2O (pH 6.6) and ALF (pH 4.5) no degradation was observed. However, exposure of SiNPs to FBS, HS, and cMEM and a pH ~ 7.4 lead to degradation, which thus is likely enhanced by the portfolio of molecules that are able to bind and complex lower molecular weight species and ions influencing degradation equilibria. The degradation behavior observed by ThT fluorescence is in good agreement with previous results and shows the in situ applicability of the method.[30]

ThT fluorescence was furthermore observed by confocal fluorescence microscopy of human cells exposed to ThT-doped SiNPs. This may allow to track, localize, and detect potential structural changes at distinct intracellular locations in real-time. Figure 5a,b shows 27 nm ThT- and FITC-doped SiNPs

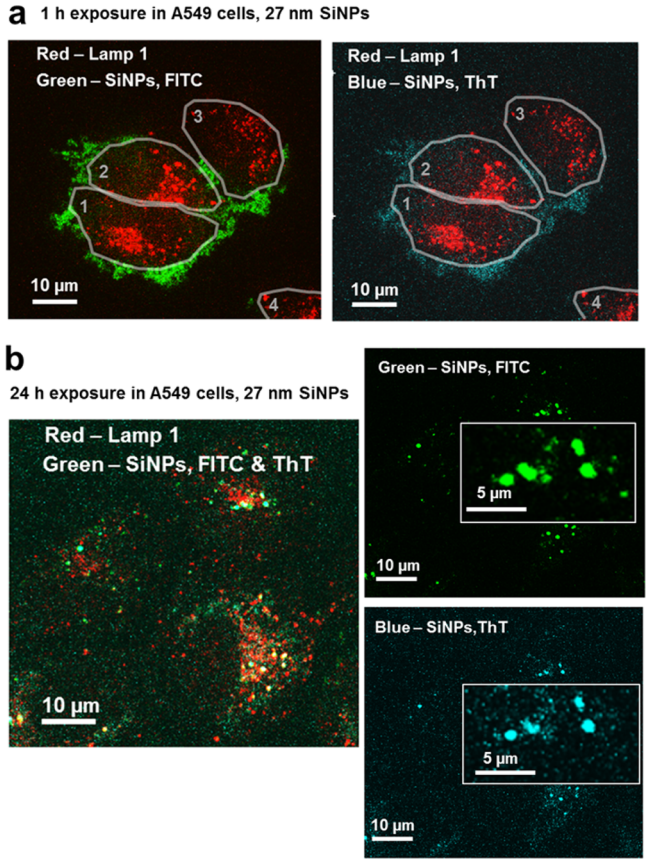

Figure 5. Tracking of 27 nm mean diameter SiNPs (doped with ThT and FITC) in confocal microscopy during exposure to human lung carcinoma epithelial A549 cells. (a) 1 h after addition of SiNPs to cells, the SiNPs can be localized in periphery of particles (FITC green, ex/em filters 488/520 nm, left image and ThT blue, ex/em filters 405/460 nm, right image). Lysosome-associated membrane glycoproteins (LAMP-1) in the cells are displayed in red; the numbered ovals mark areas occupied by individual cells and were added to guide the eyes. (b) 24 h after exposure. SiNPs can be colocalized with LAMP-1 suggesting their placement inside the cells and in lysosomes. FITC and ThT signals are visible at similar locations suggesting only no significant degradation and structural changes during intracellular processing within 24 h under the conditions of the experiments.

DOI: 10.1021/acsnano.6b01001
ACS Nano 2016, 10, 4660–4671

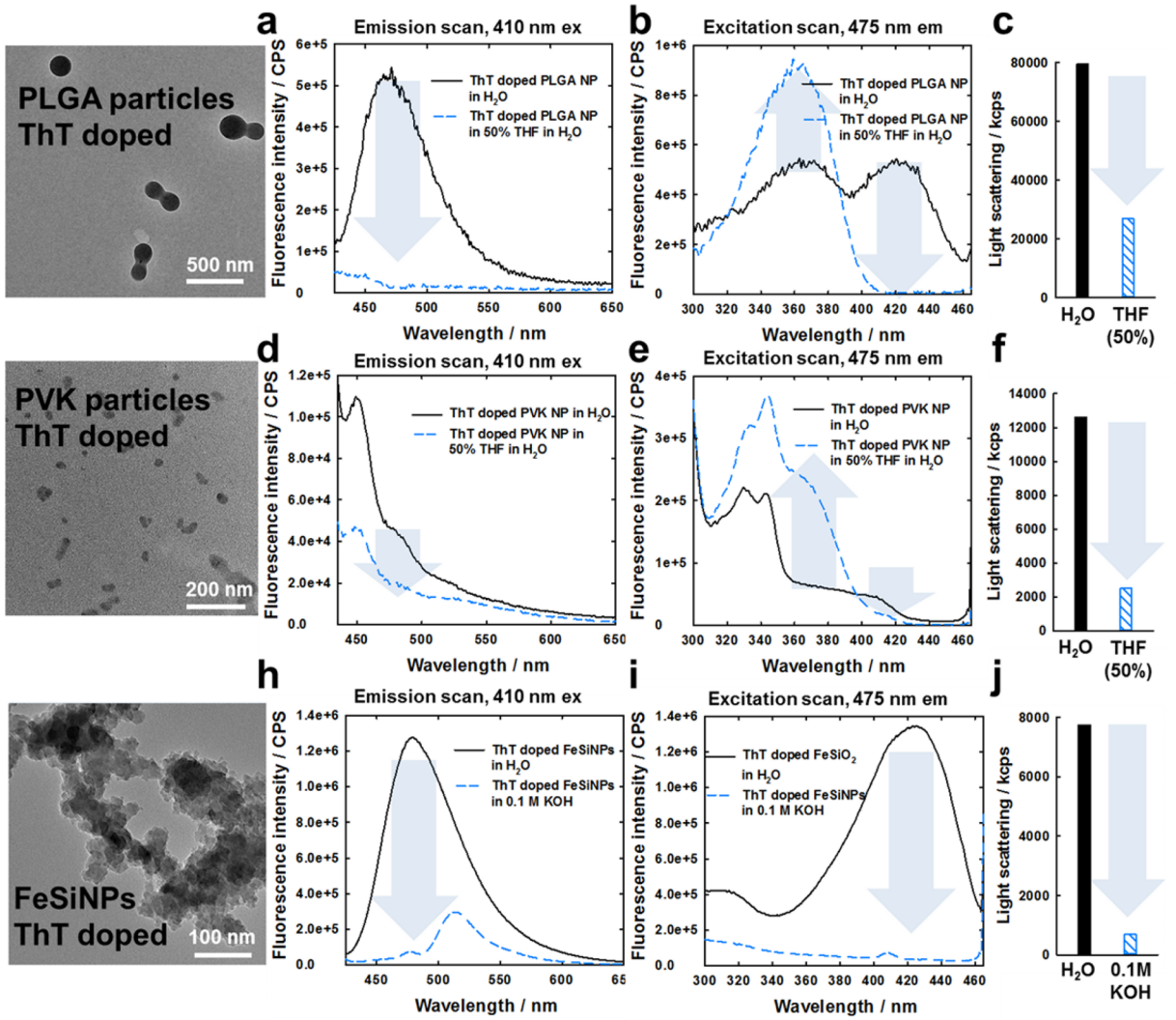

Figure 6. Sensing structural integrity of PLGA NPs, PVK NPs, and FeSiNPs doped with ThT. TEM images of as synthesized particles and fluorescence emission, excitation spectra, and light scattering and under degrading and nondegrading condition are given for PLGA NPs in (a), (b), and (c), respectively, in (d), (e), and (f) for PVK NPs, and in (h), (i), and (j) for FeSiNPs particles. The data confirms that ThT can be used as a sensor for structural integrity in different materials. Further particle characterization can be found in Figure S15.

exposed to A549 cells. Measurements of ThT and FITC signals were conducted 1 and 24 h after exposure. After 24 h, the SiNPs can be colocalized with LAMP-1 lysosomal stain, suggesting their presence in lysosomes as commonly observed for many nanomaterials.[7] Signals of both, FITC (ex/em 488/520 nm), and ThT (ex/em 405/460 nm) can be obtained. This suggests that no major degradation occurred within the experimental conditions and correlates well with the fact that silica particles are surprisingly stable in lysosomes due to their low pH (pH ∼ 4.5). SiNPs did furthermore not degrade when exposed to artificial lysosomal fluid likely due to the lower pH in lysosomes stabilizing the SiNP integrity (Figure 4a).[36] Interestingly, although SiNPs degrade in cell medium and serum, uptake into lysosomes seem to reduce or inhibit their degradation, which confirms the importance of tracking intracellular processing for understanding nanoparticle degradation. A few technical aspects need to be considered. We found that with our microscope, particles containing only FITC are not detectable in the channel used to record the ThT signal (or gave a much lower signal) although ex/em spectra of ThT and FITC slightly overlap (data not shown). This is necessary to distinguish the two signals and depends on the individual excitation lasers and emission filters. We recommend using a fluorophore with ex/em spectra that do not overlap in the with ThT spectra, for example, RITC, if artifacts occur. The methodology proved to be robust and easily applicable to cell culture providing a tool for simultaneously following structural changes without further sample preparation but further points need careful observation. A decrease of ThT fluorescence suggests degradation in an isolated system. However, cells are "open systems" and exchange with the environment. Thus, particle export or dilution by cell division can also cause the signal to disappear and should be considered and tracked.[4] We thus stress the importance of dual or multiple labeling with a fluorophore nonsensitive toward degradation, here, FITC that is colocalized with ThT. If the ThT signal disappears and the fluorescence of the reference fluorophore remains, degradation is likely and can in this way provide spacial and in situ information on the degradation status and location of nanoparticles in single cell compartments. Furthermore, in the case of degradation, it should be considered that all degradation products (including ThT) may impact cells and

DOI: 10.1021/acsnano.6b01001
ACS Nano 2016, 10, 4660−4671

organisms. ThTs' toxicity is considered low but not fully explored yet, although, positive effects like lifespan-expanding properties have been observed and cytotoxicity at low doses is marginal. (IC_{50} values for K562 cells reported by Darghal et al. are <0.3 μM ThT. For comparison, a maximum of 0.2 μM ThT can be released from 65 nm SiNPs synthesized with 0.7% ThT compared to TEOS when used at a concentration of 0.1 μg mL^{-1} and according to the ThT loading reported in Figure 1.)[26,37] Radiolabeled ThT derivates have been used for in vivo imaging of amyloids.[38] The radioactive decay, however, compared to ThT fluorescence does not depend on the molecular rotation of ThT and would thus not reflect particle integrity directly. In vivo imaging using ThT fluorescence is subject to the general limitations in fluorescence-based-in vivo-imaging (high background tissue absorbance, low penetration depths).[39] In small rodents, however, and by replacing ThT with molecular rotors that emit in near-infrared region while showing the same response toward material degradation as ThT, the approach may provide sufficient intensities. However, it is clear that on the cellular and biomolecular level, nanoparticle degradation is far from being understood, and the easy-to-apply labeling technique presented here may shed light on important reaction cascades in addition or in advance of in vivo investigations.

ThT-Doped PLGA, PKA, and Iron-Doped SiNPs. To prove if the concept is limited to silica or if it is also applicable to other material matrices, we incorporated ThT noncovalently into PLGA and PKA nanoparticles with similar result (Figure 6a–f). PLGA NPs have great potential as drug carriers due to their biocompatibility. Figure 6a,b shows that ThT doping of PLGA particles leads to the establishment of shifted and characteristic ThT fluorescence at 475 nm when rotation is blocked (not seen in nondoped PLGA particles, Figure S13), suggesting entrapment of ThT in the polymer matrix. The fluorescent signal at 475 nm disappears when adding solvent tetrahydrofuran (THF), which expectedly breaks up the PLGA particles into its polymer components. The degradation of the PLGA particles was confirmed by a drop in light scattering (Figure 6c). Also, in the excitation spectra, the characteristic peak at a wavelength of 410–425 nm for entrapped ThT with no rotational freedom disappears upon degradation and the peak at around 350–360 nm characteristic for free ThT in solution increases. The latter may confirm the regaining of the rotational freedom of ThT, but a fluorescence increase is also observed when THF is added to free ThT molecules, which complicates the direct relation of the peak increase to rotational freedom of ThT. Similarly, the ThT signal at 475 nm of free ThT molecules in THF increases slightly compared to water. This, on the other hand, strongly confirms that the signal drop at 475 nm is due to particle degradation and not due to solvent effects on ThT which would have caused a signal increase. Although less pronounced, a similar behavior can be found when ThT is included into PVK NPs. PVK is a fluorescent, semiconducting polymer with applications in biosensing and electronics.[40] PVK NPs modified with ThT have, next to their intrinsic fluorescence peaks, the characteristic emission peaks at 475 nm and nondoped particles do not show these peaks (FigureS13), suggesting entrapment of ThT in the polymer matrix. THF is solvent for PVK and thus degrades the particles (by either swelling or dissolution in polymer components; a decrease of light scattering suggests disassembly into smaller fragments; Figure 6f). The degradation is followed by signal decrease in excitation and emission spectra suggesting change of ThT's rotational properties.

Iron doping was shown to increase SiNPs degradation rates.[18] Doping with metal ions influences the material matrix and the microenvironment in the particles, which finally leads to the altered degradation behavior. To prove whether iron-doping has an influence on the fluorescence of entrapped ThT, we synthesized SiNPs simultaneously doped with iron and ThT (FeSiNPs). Figure 6h–j prove that FeSiNPs show the characteristic emission peak of entrapped ThT at 475 nm in their fluorescence spectra and the peak disappears upon particle degradation in 0.1 M KOH. According to the findings of Mitchell et al., we also observed that FeSiNPs degrade faster than non-Fe-doped SiNPs that were synthesized under same conditions but without iron addition (Figure S14).[18] Further characterization (DLS and TEM) of PLGA, PVK, and FeSiNPs particle suspensions can be found in Figure S15. During synthesis of PLGA particles, introduction of negatively charged carboxyl groups at the intrinsically aminated and positively charged chitosan used in PLGA particle synthesis, resulting in higher ThT loading (data not shown). Also, the negatively charged silica matrix led to high loadings of the positively charged ThT molecule suggesting that a negatively charged material matrix is beneficial for ThT incorporation. The experiments give evidence that ThT can be incorporated into different material types (four material variations tested here) and obtaining the characteristic emission peak at 475 nm suggesting that the process is material-independent. ThT always establishes a red-shifted fluorescence with a maximum at about 475 nm and micromechanical blocking of the molecular rotation due to entrapment seems to cause the effect.

CONCLUSIONS

Our manuscript introduces the concept of using molecular rotors for sensing integrity of nanoparticles in bionanoscience. The successful control of the relaxation pathways of the molecular rotor ThT by incorporation into different types of nanoparticle matrices is observed and described in detail. Entrapment into a nanoparticle matrix leads to strongly red-shifted fluorescence emission and excitation spectra suggesting inhibition of the molecular rotation of ThT by locking it in the material matrix. Upon nanoparticle degradation, ThT regains rotational freedom, which results in decreased fluorescence emission over up to three magnitudes. The shifted fluorescence signals sensitively reflect the integrity of the nanoparticles and allow monitoring nanoparticle structural changes. Nanoparticle integrity was thus easily sensed in biological media and serum, and it was possible to distinguish structural differences of SiNPs (particle sizes, core–shell structures) from altered degradation kinetics using ThT fluorescence. Confocal microscopy of ThT-doped SiNPs after exposure to cells provides evidence for the opportunity to track structural integrity of ThT-labeled nanoparticles in situ and in distinct cellular locations. Thus, we suggest molecular rotors such as ThT as multiplatform-compatible, complementary tools and essential future compartments of multiple labeled nanoparticles in bionanoscience to easily track structural features and structural integrity on cell and biomolecular level.

METHODS

Materials. TEOS (tetraethyl orthosilicate, 99%), APTMS ((3-aminopropyl)trimethoxysilane, 97%), FITC (fluorescein

DOI: 10.1021/acsnano.6b01001
ACS Nano 2016, 10, 4660–4671

isothiocyanate isomer I, 98%), RITC (Rhodamine B isothiocyanate, mixed isomers), ThT (thioflavin T), KOH (potassium hydroxide), methanol (99.9%), ammonium hydroxide (26%), PLGA (poly(lactic-*co*-glycolic acid, lactide:glycolide (65:35), 40 000−75 000 Da), ethyl acetate (≥99.5%), chitosan (from shrimp shells, ≥75%, deacetylated), poly(9-vinylcarbazole) (PVK, ∼1 100 000 Da), and tetrahydrofuran (THF) were purchased from Sigma-Aldrich, Ireland; ethanol (99.9%) from Merck, Germany; MEM (Minimum Essential Media) and FBS (fetal bovine serum) were purchased from Gibco, Life Technologies, Ireland; iron(III) ethoxide (99.6%) from Santa Cruz Biotechnology. Water used in all experiments was ultrapure water obtained by a Milli-Q purification system (Millipore Corporation, Ireland).

Synthesis of SiNPs. The synthesis of SiNPs was adapted from Mahon et al. and modified by the inclusion of ThT.[30] As an initial step, 0.91 g of ammonium hydroxide (26%) in 25 mL of ethanol (99.9%) were mixed. ThT was dissolved in 0.5 mL of ethanol in the indicated amounts, which are relative to the TEOS concentration (e.g., 6 mg for 0.7 wt %) and immediately given to the reaction. For doping with FITC or RITC, 0.125 mL of a conjugate solution was added subsequently (conjugate: 2 mg of FITC or RITC, respectively, 1 mL of ethanol, 10 μL of APTMS mixed and incubated in the dark for 4 h), which is 0.03 wt % relative to the added amount of TEOS. The solution was stirred for 3 min followed by addition of 0.91 mL of TEOS and stirred overnight at 25 °C at 700 rpm. Smaller particle sizes were adjusted by supplementing ethanol with methanol in the indicated percentages (by volume) in the initial step. Purification after synthesis to remove unreacted precursors and to transfer SiNPs into H_2O was either done by separating SiNPs by centrifugation and repeated washing steps (when particles >30 nm) or, when SiNPs expected to be <30 nm (high methanol concentration), by adding 15 mL of H_2O to the reaction and evaporating ethanol or methanol, respectively, under reduced pressure followed by gel permeation chromatography using a Sephadex P25 column. Washing was done by centrifugation at 20 000 rcf for 25 min, the supernatant was removed, the pellet was redispersed in 25 mL of ethanol by bath sonication, which was followed by three washing steps with 25 mL of H_2O each and final redispersion in H_2O. Afterward, an optional shell on the particle surface was synthesized to provide better particle stability, reduce dye leaking, and obtain a defined surface chemistry. If particles without shells were used in the experiments, it is specifically stated in the figure caption. For obtaining the shell, a suspension of SiNPs in H_2O was heated to 90 °C and 32.8 μL of TEOS were added per square meter of particle surface area, which was calculated from the added particle concentration, from the mean diameter from DCS measurements, and by assuming spherical particles. This corresponds to ∼20 monolayer TEOS on the particle surface. After 3 h of reaction particles have been washed three times by repeated centrifugation and resuspension in water or by gel permeation chromatography. Description of quantification of dyes in SiNPs can be found in Supporting Information.

Iron-doped SiNPs (SiFeNPs) and ThT have been synthesized by adding 2.844 mL of a 20 mg mL^{-1} iron(III) ethoxide solution, prepared by sonication-assisted dissolution of 20 mg of iron(III) ethoxide in 1 mL of anhydrous ethanol, into 25 mL of ethanol (99.9%) with 0.91 g of ammonium hydroxide (26%) and 6 mg of ThT. Then, 0.91 mL of TEOS was added and proceeded as described for SiNP synthesis above. A molar ratio of iron(III) ethoxide and TEOS was kept 0.073:1 as described earlier in the publication of Mitchell et al.[18]

ThT-doped poly(lactic-*co*-glycolic acid) (PLGA) particles have been synthesized by modifying the synthesis of Taetz et al.[41] In brief, a 20 mL aliquot was mixed with 3 mg mL^{-1} chitosan and 10 mg mL^{-1} poly(vinyl alcohol) for 30 min at RT under magnetic stirring. Then 20 mg mL^{-1} succinic anhydride were added and pH adjusted to pH 7 using 3 M NaOH (solution 1). PLGA (20 mg/mL) was dissolved in 20 mL of ethyl acetate (solution 2). Solutions 1 and 2 were magnetically stirred at RT for 2 h. Solution 1 was then filtered through a 0.45 μm syringe filter. To solution 2, 60 μL of a 50 mg mL^{-1} ThT solution in ethanol were added. Then, 5 mL of solution 2 were added dropwise to 5 mL of filtered solution 1. The emulsion was stirred at 1000 rpm for 1 h. Afterward, it was homogenized using an UltraTurrax T25 (IKA, Germany) at 13 500 rpm for 15 min. The homogenized emulsion (10 mL) was diluted by adding 17 mL of water under constant stirring. Remaining ethyl acetate was evaporated by continuous stirring overnight at room temperature followed by evaporation at 70 °C for 4 h. The particles were washed as described above using centrifugation at 10 000 rcf for 1 min.

ThT-doped poly(9-vinylcarbazole) (PVK) nanoparticles were prepared by a reprecipitation method. A 0.2 mg mL^{-1} solution of PVK was prepared by dissolving 1 mg of PVK granules in 5 mL of THF with stirring for an hour. First, 0.4 mg of ThT was dissolved in 0.2 mL of MeOH and 1.8 mL of THF were added to achieve a 0.2 mg mL^{-1} solution. Then, 0.1 mL of PVK/THF solution, 0.05 mL (50 wt %) ThT/MeOH/THF solution were mixed with 1.85 mL of THF and quickly injected into 8 mL of deionized water in a round-bottom flask while applying sonication over 3 min in order to improve mixing and increase the rate of polymer chain collapse. Following this, the resulting mixture was placed onto a rotor evaporator for 60 min in order to remove the organic solvent under reduced pressure at room temperature. After removal the organic solvent, approximately 7 mL of solution containing PVK nanoparticles remained in the round-bottomed flask.

Degradation Experiments. *Degradation in KOH.* First, 500 μL of 1 M KOH and 25 μL of 2.5 mg mL^{-1} of SiNPs were mixed and added to a cuvette. The kinetic measurement of the nanoparticles was started such that there is no lag between the addition of nanoparticles and start of the measurement using a FluoroLog 3 (Horiba, Ireland). For degradation of FeSiNP nanoparticles, 500 μL of 0.1 M KOH was mixed with 25 μL of 0.724 mg mL^{-1} nanoparticles and added to the cuvette. As control, SiNPs without FITC were used at the same concentration. Fluorescence measurements were repeated with an interval of 1 min between each set of measurement, until ThT fluorescence intensity remained constant. For baseline correction, KOH solutions were measured and subtracted from fluorescence values of the nanoparticles. The degradation was also followed using DLS, where the count rate of scattered light was recorded over the same time period as the fluorescence measurements.

Degradation in Biological Media. ThT-doped SiNPs with and without shell and ThT molecues as reference were exposed to water, ALF, cMEM (phenol red-free MEM supplemented with 10 vol % FBS), FBS, ALF, and HS for 52 h at 37 °C. ALF was prepared according to Beeston et al.[42] Next, 100 μL of 0.5 mg mL^{-1} of nanoparticles was added to 400 μL of the different media, so that the final concentration is 0.1 mg mL^{-1}. A ThT stock solution was prepared in water at a concentration of 0.35

DOI: 10.1021/acsnano.6b01001
ACS Nano 2016, 10, 4660−4671

μg mL^{-1}. Then, 100 μL of ThT solution was added to 400 μL of media with final concentration of 0.07 μg mL^{-1} of ThT in media which corresponds the amount of ThT that is incorporated in 0.1 mg mL^{-1} of particles. Fluorescence spectra were recorded immediately after mixing (time 0 h) and after 6, 24, and 52 h incubation. The solutions were kept at 37 °C on a shaker at 600 rpm between the measurements. The solutions were sonicated for 3 s before each time point measurements. Fluorescence spectra of H_2O, ALF, cMEM, FBS, and HS without particles left at 37 °C for the same time interval were subtracted from fluorescence signals of the samples for background correction.

Degradation of PLGA and PVK Nanoparticles. Degradation study of ThT-doped and nondoped PLGA and PVK nanoparticles was done in 50 vol % THF (in water) and water as reference. Then, 100 μL of 1 mg of PLGA particles in water were mixed with 100 μL of water or 50 vol % THF and was left shaking for 2 h at 600 rpm at room temperature followed by determination of fluorescence profiles. The fluorescence of ThT in water and 50 vol % THF at 1.4 μg mL^{-1} was recorded as a reference. The baselines, water and 50 vol % THF without particles, were subtracted from the fluorescence profiles of the samples.

UV−Vis Spectroscopy. UV−vis spectra were recorded on a Varian's Cary6000i spectrophotometer (Agilent Technologies, Ireland) using a quartz cuvette with a path length of 1 cm at a typical SiNP concentration of 500 μg mL^{-1}.

Fluorescence Spectroscopy. Fluorescence spectroscopy was performed in a FluoroLog 3 fluorimeter (Horiba, Ireland), typically, at a concentration of 119 μg mL^{-1} of doped SiNPs or at concentrations stated above. Usually emission spectra were recorded for excitation at 347, 410, 425, and 480 nm and the excitation spectra for fixed emission wavelengths at 440, 475, and 520 nm with a slit width of 5 nm.

Gel Electrophoresis. Gel electrophoresis was performed to detect particle dissolution and observation of free dye entering the gel as described by Mahon et al.[30] Therefore, typical SDS-PAGE gels were prepared having a 4% acrylamide stacking gel and a 10% separation gel and gels were run in TRIS buffer for 45 min at 130 V. After treatment in KOH solution, samples were neutralized before loading into the gel to avoid any effects of KOH on the gel porosity.

Dynamic Light Scattering. Dynamic Light Scattering (DLS) measurements were carried out at a typical nanoparticle concentration of 50 μg mL^{-1} in a 1 mL of polystyrene or glass cuvette. Measurements are an average of three individual runs with 10−15 accumulations per run. Samples were analyzed on a Malvern Nanosizer ZS Series (Malvern, Ireland) at a temperature of 25 °C.

Differential Centrifugal Sedimentation. Differential centrifugal sedimentation (DCS) was carried out using a CPS disc centrifuge DC24000 (CPS Instruments Inc., U.K.) in which an 8−24 w/w % sucrose-based gradient in Milli-Q water was applied. Measurements were conducted at a speed of 18 000 rpm. Calibration was performed using poly(vinyl chloride) (PVC) standard (0.476 μm, Analytik Ltd., U.K.). Calibration was carried out before each measurement using 0.1 mL of the standard; similarly, 0.1 mL of each sample was injected for the analysis using a calibrated syringe (Hamilton GASTIGHT, Hamilton, U.K.) with an accuracy of ±1% within the injected volume.

Transmission Electron Microscopy. Transmission electron microscopy (TEM) micrographs of SiNPs were obtained in a FEI Tecnai G2 20 Twin microscope (FEI, Inc., The Netherlands) at an accelerating voltage of 200 kV. Then, 5 μL of diluted SiNPs suspensions were dried and analyzed on Formvar/Carbon copper grids (300 mesh, Ted Pella Inc., U.K.).

Cell Tests and Confocal Fluorescence Microscopy. *Cell Culture.* Human lung carcinoma epithelial A549 cells (ATCC-CCL-185) were seeded at a density of 4 × 105 cells per well in 6-well plates (Greiner Bio-One GmbH, Germany) where previously sterilized coverslips had been placed. The plates were incubated in a humidified incubator at 37 °C in 5% CO_2 in MEM (with additional L-Glutamine) supplemented with 10% fetal bovine serum (FBS), 1% penicillin/streptomycin (Invitrogen, Ireland), and 1% MEM nonessential amino acids (HyClone, GE Healthcare, U.K.) to obtain complete medium (cMEM) for 24 h before exposing to the nanoparticle dispersions.

Nanoparticle Exposure. SiNPs were resuspended to a concentration of 100 μg mL^{-1} in cMEM immediately prior to exposure. Culture media was then removed from the wells and colloidal exposure solution was added to the relevant wells. cMEM was added to wells to be used as negative controls. Cells were incubated with nanoparticles in a humified incubator at 37 °C with 5% CO_2; following a 4 h exposure, the test medium was removed and the cell monolayers were washed twice with Dulbecco's Phosphate-Buffered Saline DPBS (DPBS, Gipco, Ireland), fresh cMEM was then added to the cells which were further grown for 1 and 24 h.

Confocal Imaging. Cells were fixed with 4% formalin for 15 min at room temperature and subsequently permeabilised with Saponin. A 1:10 saponin solution was added to the plates for 15 min; the permeabilization solution was then removed and the cell monolayer was washed three times with DPBS. Unspecific sites were then blocked for 30 min using a 1% BSA + 0.005% saponin solution in DPBS, followed by three DPBS washes. Cells were incubated overnight at 4 °C with anti-LAMP-1 primary antibody (Thermo Scientific, Ireland) in blocking solution. Following the three washes, the cells were incubated with anti-LAMP-1 Red secondary antibody (Thermo Scientific, Ireland) (ex/em 561/633 nm) for 30 min at room temperature then washed with DPBS three times. Images were acquired in a live cell imaging chamber (37 °C, 5% CO_2), using a spinning disc confocal microscope system incorporating a CSU-X1 spinning disc unit (Yokogawa Electric Corporation, Japan), an iXon DU-897-BV EMCCD camera (Andor, U.K.), mounted on a Nikon Ti inverted microscope (Nikon, Ireland). Images were acquired with a 100× oil immersion objective, numerical aperture 1.40. Laser lines at 405, 488, and 560 nm were used to excite the ThT, FITC, and LAMP-1, respectively. ThT emission was collected using a monochromatic 448/20 nm filter and FITC with 505−530 nm band-pass filter. Image reconstruction was performed using Imaris Software (Bitplane, version 7.4.2).

ASSOCIATED CONTENT

Supporting Information

The Supporting Information is available free of charge on the ACS Publications website at DOI: 10.1021/acsnano.6b01001.

Additional experimental details, DCS of core−shell particles, further characteristics of ThT-, FITC-, and RITC-doped SiNPs and SiNPs synthesized with varying methanol/ethanol ratios, increased detectability of ThT-

DOI: 10.1021/acsnano.6b01001
ACS Nano 2016, 10, 4660−4671

doped SiNPs in DCS, degradation of ThT- and RITC-doped SiNPs in 1 M KOH, comparison of SiNPs exposure to 1 M KOH and H_2O, influence of 1 M KOH on ThT, FITC, and RITC fluorescence. Blue shift of ThT fluorescence during degradation. ThT fluorescence and light scattering of SiNPs no shell 0.1 M KOH. Influence of biological media on free ThT, comparison of SiNPs with and without shell in biological media. Influence of Fe-doping on SiNPs degradation kinetics. Additional characterization of ThT-doped PLGA, PVK, and FeSiNPs by TEM and DLS. Fluorescence spectra of bare PVK and PLGA particles. (PDF)

AUTHOR INFORMATION

Corresponding Authors

*E-mail: kenneth.a.dawson@cbni.ucd.ie.
*E-mail: mederf@gmx.de.

Author Contributions

§These authors contributed equally.

Notes

The authors declare no competing financial interest.

ACKNOWLEDGMENTS

F.M. gratefully acknowledges the support by the German Research Foundation (DFG) within the "Forschungsstipendium" ME 4296/1-1. S.T. would like to acknowledge the Irish Research Council (G01PG/2013/104). L.F. acknowledges the Irish Research Council for funding the Embark scheme (RS/2012/190). A.A. acknowledges the Princess Nourah Bint Abdulrahman University Project Ref: IR10177, ID: 1056571209. We acknowledge the Seventh Framework Programme, FutureNanoNeeds, grant agreement no. 604602 and the Science Foundation Ireland Principal Investigator Award "Biological Identity of Nanoparticles Dispersed in Biological Media", project ID: 12/IA/1422. The authors acknowledge the Imaging Core facility at the Conway Institute, UCD.

REFERENCES

(1) Moghimi, S. M.; Peer, D.; Langer, R. Reshaping the Future of Nanopharmaceuticals. *ACS Nano* **2011**, *5*, 8454−8458.
(2) De, M.; Ghosh, P. S.; Rotello, V. M. Applications of Nanoparticles in Biology. *Adv. Mater.* **2008**, *20*, 4225−4241.
(3) Nel, A. E.; Maedler, L.; Velegol, D.; Xia, T.; Hoek, E. M. V.; Somasundaran, P.; Klaessig, F.; Castranova, V.; Thompson, M. Understanding Biophysicochemical Interactions at the Nano-Bio Interface. *Nat. Mater.* **2009**, *8*, 543−557.
(4) Kim, J. A.; Aberg, C.; Salvati, A.; Dawson, K. A. Role of Cell Cycle on the Cellular Uptake and Dilution of Nanoparticles in a Cell Population. *Nat. Nanotechnol.* **2011**, *7*, 62−68.
(5) Park, J.-H.; Gu, L.; von Maltzahn, G.; Ruoslahti, E.; Bhatia, S. N.; Sailor, M. J. Biodegradable Luminescent Porous Silicon Nanoparticles for in vivo Applications. *Nat. Mater.* **2009**, *8*, 331−336.
(6) Tengood, J. E.; Alferiev, I. S.; Zhang, K.; Fishbein, I.; Levy, R. J.; Chorny, M. Real-Time Analysis of Composite Magnetic Nanoparticle Disassembly in Vascular Cells and Biomimetic Media. *Proc. Natl. Acad. Sci. U. S. A.* **2014**, *111*, 4245−4250.
(7) Bertoli, F.; Davies, G.-L.; Monopoli, M. P.; Moloney, M.; Gun'ko, Y. K.; Salvati, A.; Dawson, K. A. Magnetic Nanoparticles to Recover Cellular Organelles and Study the Time Resolved Nanoparticle-Cell Interactome Throughout Uptake. *Small* **2014**, *10*, 3307−3315.
(8) Albanese, A.; Walkey, C. D.; Olsen, J. B.; Guo, H.; Emili, A.; Chan, W. C. W. Secreted Biomolecules Alter the Biological Identity and Cellular Interactions of Nanoparticles. *ACS Nano* **2014**, *8*, 5515−5526.
(9) Kreyling, W. G.; Abdelmonem, A. M.; Ali, Z.; Alves, F.; Geiser, M.; Haberl, N.; Hartmann, R.; Hirn, S.; de Aberasturi, D. J.; Kantner, K.; Khadem-Saba, G.; Montenegro, J. M.; Rejman, J.; Rojo, T.; de Larramendi, I. R.; Ufartes, R.; Wenk, A.; Parak, W. J. In vivo Integrity of Polymer-Coated Gold Nanoparticles. *Nat. Nanotechnol.* **2015**, *10*, 619−623.
(10) Llop, J.; Jiang, P.; Marradi, M.; Gómez-Vallejo, V.; Echeverría, M.; Yu, S.; Puigivila, M.; Baz, Z.; Szczupak, B.; Pérez-Campaña, C.; Mao, Z.; Gao, C.; Moya, S. E. Visualisation of Dual Radiolabelled Poly(Lactide-Co-Glycolide) Nanoparticle Degradation in vivo Using Energy-Discriminant Spect. *J. Mater. Chem. B* **2015**, *3*, 6293−6300.
(11) Larson, D. R.; Ow, H.; Vishwasrao, H. D.; Heikal, A. A.; Wiesner, U.; Webb, W. W. Silica Nanoparticle Architecture Determines Radiative Properties of Encapsulated Fluorophores. *Chem. Mater.* **2008**, *20*, 2677−2684.
(12) Ow, H.; Larson, D. R.; Srivastava, M.; Baird, B. A.; Webb, W. W.; Wiesner, U. Bright and Stable Core−Shell Fluorescent Silica Nanoparticles. *Nano Lett.* **2005**, *5*, 113−117.
(13) Shahabi, S.; Treccani, L.; Dringen, R.; Rezwan, K. Dual Fluorophore Doped Silica Nanoparticles for Cellular Localization Studies in Multiple Stained Cells. *Acta Biomater.* **2015**, *14*, 208−216.
(14) Phillips, E.; Penate-Medina, O.; Zanzonico, P. B.; Carvajal, R. D.; Mohan, P.; Ye, Y.; Humm, J.; Gönen, M.; Kalaigian, H.; Schöder, H.; Strauss, H. W.; Larson, S. M.; Wiesner, U.; Bradbury, M. S. Clinical Translation of an Ultrasmall Inorganic Optical-PET Imaging Nanoparticle Probe. *Sci. Transl. Med.* **2014**, *6*, 260ra149.
(15) Argyo, C.; Weiss, V.; Bräuchle, C.; Bein, T. Multifunctional Mesoporous Silica Nanoparticles as a Universal Platform for Drug Delivery. *Chem. Mater.* **2014**, *26*, 435−451.
(16) Tang, L.; Cheng, J. Nonporous Silica Nanoparticles for Nanomedicine Application. *Nano Today* **2013**, *8*, 290−312.
(17) Suteewong, T.; Sai, H.; Hovden, R.; Muller, D.; Bradbury, M. S.; Gruner, S. M.; Wiesner, U. Multicompartment Mesoporous Silica Nanoparticles with Branched Shapes: An Epitaxial Growth Mechanism. *Science* **2013**, *340*, 337−341.
(18) Pohaku Mitchell, K. K.; Liberman, A.; Kummel, A. C.; Trogler, W. C. Iron(III)-Doped, Silica Nanoshells: A Biodegradable Form of Silica. *J. Am. Chem. Soc.* **2012**, *134*, 13997−14003.
(19) Hao, X.; Hu, X.; Zhang, C.; Chen, S.; Li, Z.; Yang, X.; Liu, H.; Jia, G.; Liu, D.; Ge, K.; Liang, X.-J.; Zhang, J. Hybrid Mesoporous Silica-Based Drug Carrier Nanostructures with Improved Degradability by Hydroxyapatite. *ACS Nano* **2015**, *9*, 9614−9625.
(20) Cauda, V.; Schlossbauer, A.; Kecht, J.; Zürner, A.; Bein, T. Multiple Core−Shell Functionalized Colloidal Mesoporous Silica Nanoparticles. *J. Am. Chem. Soc.* **2009**, *131*, 11361−11370.
(21) Salvati, A.; Åberg, C.; dos Santos, T.; Varela, J.; Pinto, P.; Lynch, I.; Dawson, K. A. Experimental and Theoretical Comparison of Intracellular Import of Polymeric Nanoparticles and Small Molecules: Toward Models of Uptake Kinetics. *Nanomedicine* **2011**, *7*, 818−826.
(22) Barthel, A.-K.; Dass, M.; Dröge, M.; Cramer, J.-M.; Baumann, D.; Urban, M.; Landfester, K.; Mailänder, V.; Lieberwirth, I. Imaging the Intracellular Degradation of Biodegradable Polymer Nanoparticles. *Beilstein J. Nanotechnol.* **2014**, *5*, 1905−1917.
(23) He, Q.; Shi, J.; Zhu, M.; Chen, Y.; Chen, F. The Three-Stage in vitro Degradation Behavior of Mesoporous Silica in Simulated Body Fluid. *Microporous Mesoporous Mater.* **2010**, *131*, 314−320.
(24) Bergman, L.; Kankaanpää, P.; Tiitta, S.; Duchanoy, A.; Li, L.; Heino, J.; Lindén, M. Intracellular Degradation of Multilabeled Poly(Ethylene Imine)−Mesoporous Silica−Silica Nanoparticles: Implications for Drug Release. *Mol. Pharmaceutics* **2013**, *10*, 1795−1803.
(25) Kamat, N. P.; Liao, Z.; Moses, L. E.; Rawson, J.; Therien, M. J.; Dmochowski, I. J.; Hammer, D. A. Sensing Membrane Stress with near IR-Emissive Porphyrins. *Proc. Natl. Acad. Sci. U. S. A.* **2011**, *108*, 13984−13989.
(26) Alavez, S.; Vantipalli, M. C.; Zucker, D. J.; Klang, I. M.; Lithgow, G. J. Amyloid-Binding Compounds Maintain Protein Homeostasis During Ageing and Extend Lifespan. *Nature* **2011**, *472*, 226−229.

DOI: 10.1021/acsnano.6b01001
ACS Nano 2016, 10, 4660−4671

(27) Biancalana, M.; Koide, S. Molecular Mechanism of Thioflavin-T Binding to Amyloid Fibrils. *Biochim. Biophys. Acta, Proteins Proteomics* **2010**, *1804*, 1405−1412.
(28) Freire, S.; de Araujo, M. H.; Al-Soufi, W.; Novo, M. Photophysical Study of Thioflavin T as Fluorescence Marker of Amyloid Fibrils. *Dyes Pigm.* **2014**, *110*, 97−105.
(29) Hutter, T.; Amdursky, N.; Gepshtein, R.; Elliott, S. R.; Huppert, D. Study of Thioflavin-T Immobilized in Porous Silicon and the Effect of Different Organic Vapors on the Fluorescence Lifetime. *Langmuir* **2011**, *27*, 7587−7594.
(30) Mahon, E.; Hristov, D. R.; Dawson, K. A. Stabilising Fluorescent Silica Nanoparticles against Dissolution Effects for Biological Studies. *Chem. Commun.* **2012**, *48*, 7970−7972.
(31) Brinker, C. J.; Scherer, G. W. *Sol-Gel Science: The Physics and Chemistry of Sol-Gel Processing*; Academic Press: Boston, 1990; pp 99−100.
(32) Green, D. L.; Lin, J. S.; Lam, Y.-F.; Hu, M. Z. C.; Schaefer, D. W.; Harris, M. T. Size, Volume Fraction, and Nucleation of Stober Silica Nanoparticles. *J. Colloid Interface Sci.* **2003**, *266*, 346−358.
(33) Wohlleben, W. Validity Range of Centrifuges for the Regulation of Nanomaterials: From Classification to as-Tested Coronas. *J. Nanopart. Res.* **2012**, *14*, 1−18.
(34) Hackl, E. V.; Darkwah, J.; Smith, G.; Ermolina, I. Effect of Acidic and Basic pH on Thioflavin T Absorbance and Fluorescence. *Eur. Biophys. J.* **2015**, *44*, 249−261.
(35) Pourbaix, M. *Atlas of Electrochemical Equilibria in Aqueous Solutions*; National Association of Corrosion Engineers: Houston, 1974.
(36) Ehrlich, H.; Demadis, K. D.; Pokrovsky, O. S.; Koutsoukos, P. G. Modern Views on Desilicification: Biosilica and Abiotic Silica Dissolution in Natural and Artificial Environments. *Chem. Rev.* **2010**, *110*, 4656−4689.
(37) Darghal, N.; Garnier-Suillerot, A.; Salerno, M. Mechanism of Thioflavin T Accumulation inside Cells Overexpressing P-Glycoprotein or Multidrug Resistance-Associated Protein: Role of Lipophilicity and Positive Charge. *Biochem. Biophys. Res. Commun.* **2006**, *343*, 623−629.
(38) Kung, M.-P.; Hou, C.; Zhuang, Z.-P.; Zhang, B.; Skovronsky, D.; Trojanowski, J. Q.; Lee, V. M. Y.; Kung, H. F. IMPY: An Improved Thioflavin-T Derivative for in vivo Labeling of β-Amyloid Plaques. *Brain Res.* **2002**, *956*, 202−210.
(39) Rao, J.; Dragulescu-Andrasi, A.; Yao, H. Fluorescence Imaging in vivo: Recent Advances. *Curr. Opin. Biotechnol.* **2007**, *18*, 17−25.
(40) Dawson, K.; Lovera, P.; Iacopino, D.; O'Riordan, A.; Redmond, G. Multi-Colour Emission from Dye Doped Polymeric Nanotubes by Host−Guest Energy Transfer. *J. Mater. Chem.* **2011**, *21*, 15995−16000.
(41) Taetz, S.; Nafee, N.; Beisner, J.; Piotrowska, K.; Baldes, C.; Murdter, T. E.; Huwer, H.; Schneider, M.; Schaefer, U. F.; Klotz, U.; Lehr, C. M. The Influence of Chitosan Content in Cationic Chitosan/PLGA Nanoparticles on the Delivery Efficiency of Antisense 2′-O-Methyl-Rna Directed against Telomerase in Lung Cancer Cells. *Eur. J. Pharm. Biopharm.* **2009**, *72*, 358−369.
(42) Beeston, M. P.; Teun van Elteren, J.; Simon Selih, V.; Fairhurst, R. Characterization of Artificially Generated PbS Aerosols and Their Use within a Respiratory Bioaccessibility Test. *Analyst* **2010**, *135*, 351−357.

DOI: 10.1021/acsnano.6b01001
ACS Nano 2016, 10, 4660−4671